Journal of Hydrology 575 (2019) 999–1010

Contents lists available at ScienceDirect

Journal of Hydrology

journal homepage: www.elsevier.com/locate/jhydrol

Research papers

Nonstationary frequency analysis of the recent extreme precipitation events in the United States

Tue M. Vu, Ashok K. Mishra*

Glenn Department of Civil Engineering, Clemson University, Clemson, SC, USA

ARTICLE INFO

Keywords:
Nonstationary frequency analysis
Extreme precipitation
IDF curves

ABSTRACT

The intensification of the hydrologic cycle due to climate change is likely to influence the extreme precipitation characteristics (i.e., intensity, duration and frequency). These precipitation characteristics are integrated to construct Intensity-Duration-Frequency (IDF) curves that are widely used to design civil infrastructure systems. These IDF curves are typically derived based on the stationary assumption, however, the frequency and intensity of extreme precipitation events likely to become nonstationary as a consequence of climate change. During the past decades, unusual extreme precipitation events with more than thousand-year return periods were recorded in the United States. This study investigates the nonstationary nature of the most recent extreme precipitation events occurred over different durations (1-, 3- and 5-days) by incorporating time-varying covariates, such as time, maximum temperature, mean temperature, and the El Niño Southern Oscillation cycle (ENSO). The nonstationary frequency analysis for these extreme events was conducted using nonstationary Generalized Extreme Value distribution by incorporating the time-varying covariates. It was observed that most of the temporal evolution of extreme precipitation events follow the nonstationary pattern, which may be due to the increase in the magnitude of recent extreme precipitation events, especially during hurricane events. Different combination of covariates can potentially influence the nonstationary frequency analysis, and the type of covariate may differ when the accumulated period of extreme precipitation event increased. Based on the Nonstationary Extreme Value Analysis, the return periods associated with extreme precipitation events significantly reduced compared to the stationary approach.

1. Introduction

The design of major infrastructures, such as urban and highway drainage, flood barriers, hydraulic structures, sewerage systems, and dam spillways relies on magnitude and frequency of heavy precipitation events (Mishra and Singh, 2010). As a consequence, it is important to understand the spatial and seasonal distribution of extreme precipitation events. However, the spatiotemporal distribution of extreme (precipitations) vary between regions in terms of their magnitude, intensity and temporal distribution within a given time frame (Konapala et al., 2017; Mishra et al., 2009; Donat et al., 2016). Over the past six decades, there is a robust increase in the extreme daily precipitation averaged over both dry and wet regimes based on both observations and climate models (Donat et al., 2016). The existing infrastructures are often designed using Intensity-Duration-Frequency (IDF) curves based on the stationary assumption, which suggests that the behavior (e.g., statistical characteristics) of the natural hydrologic system does not change over a period of time. However, many studies suggested an increase in non-stationary nature of climate patterns (Milly et al., 2008; Katz, 2009, 2013; Villarini et al., 2009; Son et al., 2017; Sarhadi and Soulis, 2017; Risser and Wehner, 2017). Due to the change in climate patterns, the stationary assumption of IDF curves might underestimate the extreme events. Recently several studies indicated that the design storm estimated based on stationary models are lower compared to the nonstationary models (Cheng and AghaKhouchak, 2014; Mondal and Mujumdar, 2015; Wi et al., 2016; Sarhadi and Soulis, 2017; Emanuel, 2017; Agilan and Umamahesh, 2017; Pfahl et al., 2017). Over time, the divergence between stationary and nonstationary flood frequency magnitudes increases under climate change scenarios (Condon et al., 2015).

Global warming heats up the atmosphere, leading to the increase in evaporation and expansion of atmospheric water vapor content that further results in the intensification in the spatiotemporal distribution of extreme precipitation events (Neelin et al., 2017; O'Gorman and Schneider, 2009; Mishra and Singh, 2010). For each one degree Celcius increment in temperature, the extreme precipitation is observed to

* Corresponding author.
E-mail address: ashokm@g.clemson.edu (A.K. Mishra).

https://doi.org/10.1016/j.jhydrol.2019.05.090
Received 19 March 2019; Received in revised form 28 May 2019; Accepted 30 May 2019
Available online 31 May 2019

increase by about 7% as formulated by Clausius-Clapeyron equation (Westra et al., 2014, Ivancic and Shaw, 2016). In general, climate models suggest an intensification of extreme precipitation events during the 21st century (Pfahl et al., 2017), although they vary in space and time. Extreme precipitation events can cause severe flooding, property damage, potential loss of life, especially for urban areas with high population density (Mishra and Singh, 2010). Recently, there has been an increase in a number of studies on extreme precipitation events in the United States (Huang et al., 2018; Luong et al, 2017, Leng et al., 2016; Bracken et al., 2015). The trends in extreme precipitation (+2% per decade, in the top 1% of observed events) are higher than mean precipitation (+0.6% per decade) (Kunkel et al., 2013, 2008) reveals a significant shift in the tails of the distribution. Previous studies provided strong evidence that there is an upward trend in the frequency and intensity of extreme precipitation over the US (Kunkel et al., 2013).

The nonstationary frequency analysis depends on appropriate covariates, for example, based on only time-varying component (Sarhadi and Soulis, 2017; Son et al., 2017); human-induced changes based on the CO_2 concentration (Risser and Wehner, 2017); global warming in the form of global gridded temperature (Mondal and Mujumdar, 2015); urbanization based on the changes in the land use with respect to time (Agilan and Umamahesh, 2017), and large-scale climate covariates such as El Niño Southern Oscillation (ENSO), North Atlantic Oscillation (NAO) (Vasiliades et al., 2015). For example, the human-induced changes (e.g., CO_2 concentration and global warming) plays a significant role by increasing the chances of maximum 7-day accumulated precipitation during Hurricane Harvey by a factor of at least 3.5 (Risser and Wehner, 2017). These covariates have a potential influence on nonstationary behavior of climate variables (e.g., extreme precipitation), therefore identification of important covariates for the nonstationary frequency analysis is an important step.

1.1. Recent extreme precipitation events in the US

During the past three decades (1980–2018), overall 241 weather and climate related disasters impacted the USA, where each disaster resulted in economic losses exceeding $1 billion (NOAA, 2019) (Fig. 1). While drought and wildfire (dry events) are a very typical phenomenon for western contiguous United States (US) with one event per year, the number of wet events (categorized as a severe storm, tropical cyclone, flood) has dramatically increased since 2005. These numbers highlight the recent increasing trends of the occurrences of wet catastrophic events, especially for severe storm events. Statistically, the annual economic losses due to the billion-dollar weather disasters for the US have increased significantly about 5% per year (Smith and Katz, 2013), in which, the wet events have a significant contribution.

The extreme precipitations events are often associated with hurricanes and tropical storms in the US. For example, Huang et al. (2018) indicated that the main reason for the abrupt increase in extreme precipitation over the northeastern United States is due to the occurrence of the hurricane and tropical storms, and these are typically fueled by the warmer Atlantic Ocean temperature that heats up the atmospheric water vapor. Hurricanes often lead to extreme precipitation events that can cause significant damage to the US economy. For example, two major hurricanes occurred in the same year (2017) are: (a) the Hurricane Harvey which devastated Houston, Texas (August 26th-28th), followed by (b) Hurricane Irma (September 9th-11th) that caused significant damage to Florida. These two hurricanes resulted in a total economic loss for the United States in an excess of $125 billion (Aon, 2018). The natural disasters such as the Hurricanes Harvey and Irma highlighted the need for quantitative estimation of the risk of such disasters (Emanuel, 2017).

In our study, we identified six extreme precipitation events occurred in the USA during the period of 2011–2017, and these extreme events are displayed in Fig. 2 by PRISM precipitation data (Daly et al., 1994). The accumulated 3-day precipitation due to hurricane Harvey over Houston (Texas) was about 800 mm (Fig. 2a), and the 500 mm of precipitation is equivalent to a return period of 2000 years for the same location (Emanuel, 2017). Hurricane Harvey, the eighth named storm of the 2017 Atlantic hurricane season was recognized as the wettest tropical cyclone ever recorded to hit the USA (Ellenrieder, 2018) leading to the unprecedented amount of precipitation and massive inland flooding in the greater Houston area (Risser and Wehner, 2017). Hurricane Irma, a Category 5 storm (Editorial, 2017) considered to be the most powerful storm ever recorded in the Atlantic hurricane, brought massive precipitation accompanied by strong wind gusts and storm surge. The maximum precipitation occurred during hurricane Irma at Fort Pierce, FL was about 400 mm with the maximum wind gust of 230 km/h. Prior to Irma, the magnitude of extreme precipitation from a no-name storm in Louisiana (Aug 2016) was recognized as the 1000 year event which resulted in three times as much precipitation as hurricane Katrina (Samenow, 2016; NWS, 2016). This extreme precipitation in Lousiana resulted in flash flooding, river flooding and backwater flooding over a period of time. The Lousiana official reported that over 30,000 people rescued, and at least 60,600 homes had been impacted, and this event reported to have killed at least 13 people (van der Wiel et al., 2017). Another thousand-year precipitation event occurred near the coast of South Carolina in Oct 2015 (Mizzell et al., 2016; Marciano and Lackmann, 2017), that resulted in 430 mm of precipitation over four consecutive days. This extreme precipitation

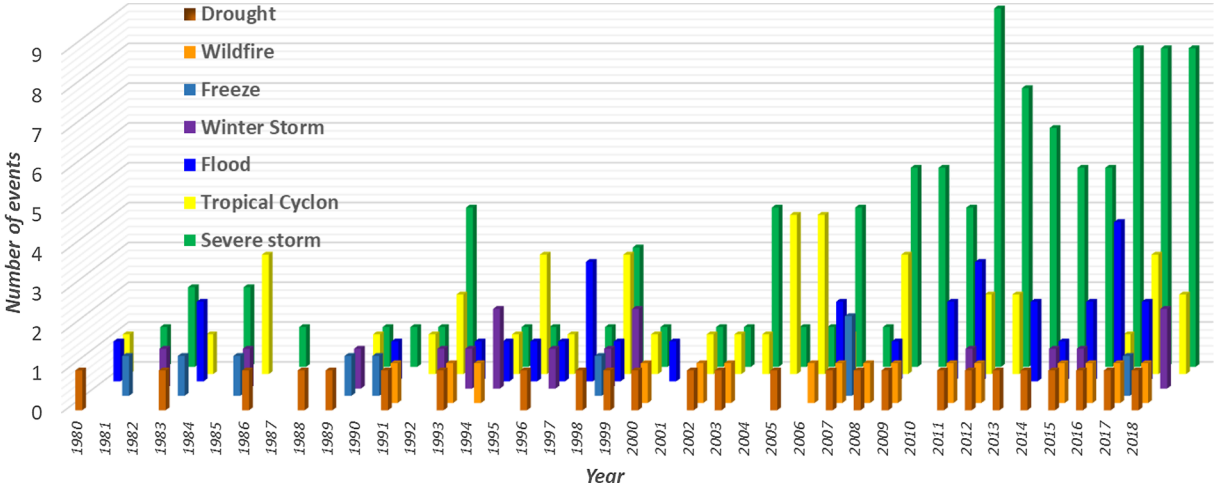

Fig. 1. Different type of extreme events that impacted USA during 1980–2018 period. [Note: The economic loss caused by individual extreme event exceeds $1 billion).

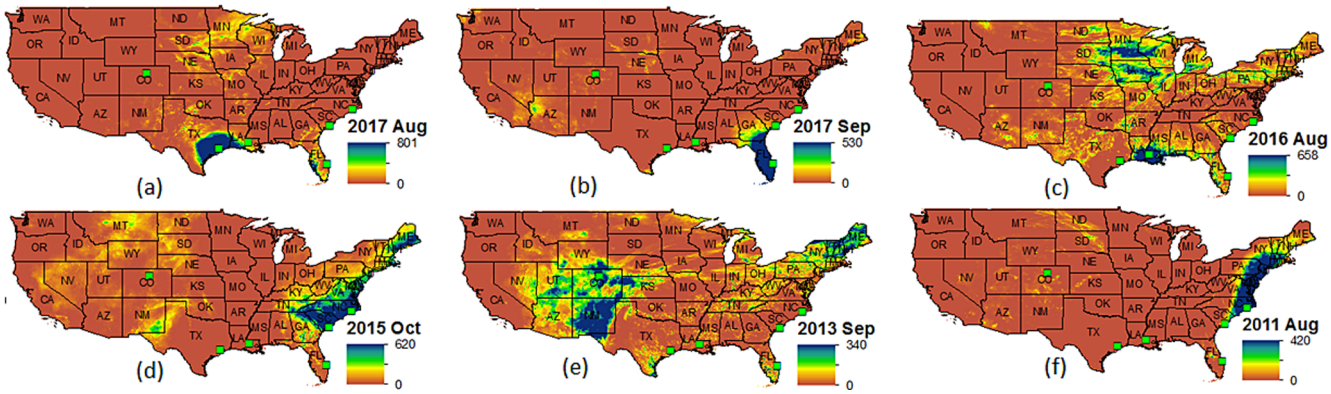

Fig. 2. Six most recent extreme (accumulated) rainfall events in the United States used in the study: (a) Houston (Texas): hurricane Harvey Aug 26th-28th 2017; (b) Florida: hurricane Irma Sep 9th-11th 2017; (c) Louisiana: Aug 11th-13th 2016; (d) Charleston (South Carolina): hurricane Joaquin Oct 1st-5th 2015; (e) Boulder (Colorado): Aug 10th-15th 2013; (f) North Carolina: Aug 27th-28th 2011. The 6 locations are highlighted in green squares in each of the plot, and they were obtained based on PRISM data sets. (For interpretation of the references to colour in this figure legend, the reader is referred to the web version of this article.)

event caused higher flood damage due to unusually high tides (due to the recent perigean spring tide) and saturated soil moisture due to the heavy precipitation in late September (CRN, 2016). The maximum daily precipitation (Sep 2013) of magnitude 230 mm recorded at Boulder, Colorado led to Front Range Flood (Yochum and Moore, 2013), which is considered to be one of the most extreme major flood disasters. The annual exceedance probability for this extreme precipitation event was as low as 1/1000 (Gochis et al., 2015; NWS, 2013). Several states in the northeastern United States witnessed severe flooding due to hurricane Irene and the remnants of Tropical Storm Lee in late August/early September 2011 that resulted in total damage of $7 billion and approximately 45 deaths (Suro et al., 2011). Among the six recent extreme event locations, Boulder is located in the Continental Subarctic climate region, and the remaining five locations are located in the Mediterranean climate region (Degu et al., 2011). These most recent catastrophic events occurred in a different part of the US at different times resulted in the major socio-economic loss.

The overall goal of this study is to: (i) identify the best covariates between time, daily maximum temperature, annual average temperature and ENSO that has potential influence on the most recent extreme precipitation events in the United States, (ii) to derive the updated return levels and return periods of these extreme precipitation events in the context of nonstationary frequency analysis, and (iii) to evaluate the perspective of nonstationary information on the return periods in order to highlight the necessity of the revised IDF curves for infrastructure designs.

2. Data and choices of covariates

2.1. Extreme values of precipitation data

The daily precipitation and maximum (minimum) temperature for the six selected locations were obtained from the Global Historical Climatology Network (GHCN) (ftp://ftp.ncdc.noaa.gov/pub/data/ghcn/daily/) (Table 1). These locations recently witnessed extreme precipitation events (discussed in Section 1.1), and the data sets are available for longer time periods with less than 1% missing value. Additional information on these selected stations are provided in Table 1, and their locations are shown in Fig. 2. Mean daily temperature value is averaged based on the maximum and minimum temperature recorded for the same day.

In general, three different methods are commonly used to identify extreme precipitation events (Mishra and Singh, 2010), and they are classified based on their amount, specific thresholds, and annual maxima values. In this study, extreme precipitation events are calculated based on the annual maximum 24 h precipitation time series. The 1-, 3-, 5-consecutive days of Annual Maximum Precipitation (AMR) time series are derived, and they are denoted by 1 day, 3 day and 5 day AMR. The 3 day AMR time series for all six selected stations and the date of occurrence of the most recent extreme events are presented in Fig. 3. Overall it was observed that the magnitude of recent extreme events is comparatively much higher than previous events.

2.2. Choices of covariates for non-stationary analysis

In this section, we provide an overview of the selected covariates and their potential influence on extreme events. The temperature can be considered as an important covariate because the warmer atmosphere is likely to hold more moisture, thereby generating a favorable condition for an increase in precipitation (Romero et al., 2011). In addition to that, based on the Clausius-Claperon relationship, a stronger relationship between daily maximum temperature and extreme precipitation events was observed compared to average temperature (Herath et al., 2018). Clausius-Clapeyron relationship also reveals the increase in saturated specific humidity in the warmer air by 6–7% per degree Kelvin of local warming in the absence of any dynamical change (Risser and Wehner, 2017). Therefore, the maximum daily temperature can be considered as an important covariate in the nonstationary analysis of extreme precipitation. In addition to that, changes in local temperature can have a significant correlation with extreme

Table 1
List of selected stations corresponding to six extreme rainfall events in the United States.

Event ID	Stations (State)	Lon	Lat	Hurricane/Storm	Event date	Data length
1	Fort Pierce (FL)	−80.35	27.44	Irma	9/17/2017	1940–2017
2	Houston Airport (TX)	−95.28	29.64	Harvey	8/17/2017	1940–2017
3	Barton Rouge Airport (LA)	−91.14	30.53	Storm	8/16/2016	1930–2017
4	Charleston Airport (SC)	−79.92	32.77	Joaquin	10/15/2015	1938–2017
5	Boulder (CO)	−105.27	39.99	Storm	9/13/2013	1918–2017
6	Bayboro (NC)	−76.81	35.13	Irene	8/27/2011	1969–2017

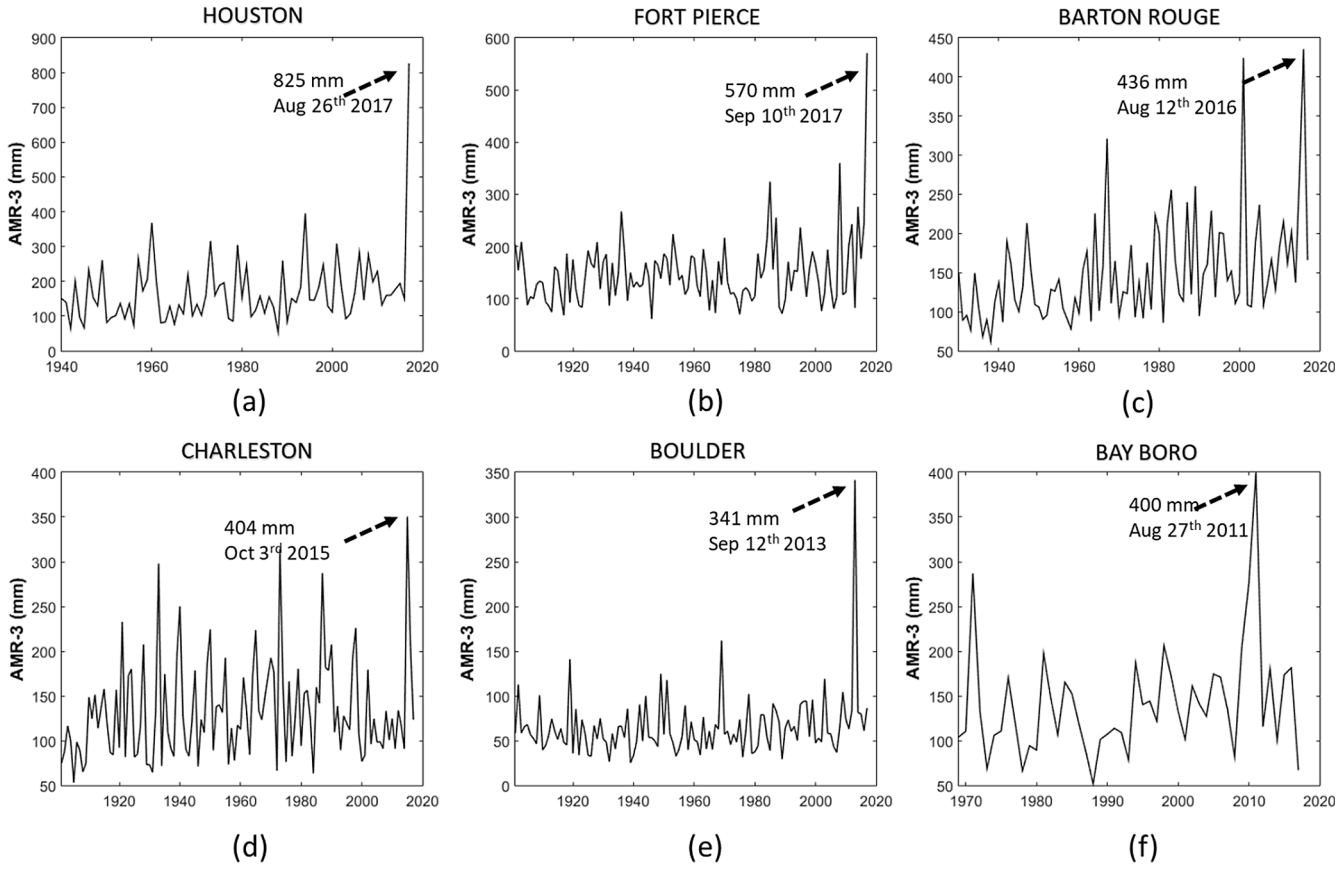

Fig. 3. Time series of 3 day AMR for six stations used in the study: (a) Houston Will Hobby airport, TX; (b) Fort Pierce, FL; (c) Barton Rouge Ryan airport, LA; (d) Charleston International Airport, SC; (e) Boulder, CO; (f) BayBoro, NC. The magnitude and date of recent extreme event for each station are shown in the figure.

precipitation intensity and frequency compared to the global process (Mondal and Mujumdar, 2015). Agilan and Umamahesh (2017) highlighted the strong correlation between change in local temperature and sub-hourly duration extreme precipitation events for a station in India. In our study, we considered the local annual average temperature as an additional covariate to study their influence on extreme precipitation events. Several studies (Sarhadi and Soulis, 2017; Son et al., 2017) included time covariate in the non-stationary analysis, and therefore it is included as an additional covariate to study the nonstationary process for the recent extreme precipitation events in the United States.

Large-scale climate indices (e.g., ENSO) likely to influence local weather conditions. ENSO (El Niño/Southern Oscillation) is a coupled ocean-atmosphere phenomenon associated with the fluctuations in the sea surface temperature located in the tropical Pacific. The extreme phases of ENSO has a potential influence on precipitation anomalies in many geographic locations around the world (Mason and Goddard, 2001), and especially it has significant influence on extreme precipitation events over the contiguous United States (Yu et al., 2017; DeFlorio et al., 2013; Schubert et al., 2008; Gershunov and Barnett, 1998; Mishra and Singh, 2010). There are several indices used to represent the phase and strength of ENSO events (Hanley et al., 2003). Typically, the commonly used indices are the regional Sea Surface Temperature (STT) in the equatorial Pacific (Niño-1 + 2, Niño-3, Niño-4, Niño-3.4). Niño 3.4 is a widely used index of ENSO activity, and it is calculated by averaging the Kaplan Extended SST anomalies (Kaplan et al., 1998) in the region comprising 5S–5 N and 170 W–120 W. Previously, Niño 3.4 was used as a covariate for modeling nonstationary precipitation (Agilan and Umamahesh, 2017; Son et al., 2017; Mondal and Mujumdar, 2015; Risser and Wehner, 2017). In this study, we selected Niño 3.4 based on Extended Reconstructed SST (ERSST) data set averaged over the November to March as an additional covariate to represent the large-scale climate phenomenon for nonstationary analysis of extreme precipitation events.

3. Methodology

3.1. Nonstationary extreme value analysis

It is often useful to study the extreme precipitation events based on longer durations (e.g., few days) due to the lag time associated between excessive precipitation and hydrologic flooding (Mishra and Singh, 2010). Therefore, the extreme precipitation values in the present study were derived based on maximum annual precipitation amounts at different time scales (1, 3, and 5 days).

The distributions of extreme values (Fisher and Tippett, 1928) include three families: Gumbel, Fréchet, and Weibull. All three families are combined into the generalized extreme values distribution (GEV) (Jenkinson, 1955). The GEV was used to derive both stationary and nonstationary models. The cumulative distribution function (CDF) of the GEV family has the functional form (Jenkinson, 1955):

$$G(z) = \exp\left\{-\left[1 + \xi\left(\frac{z-\mu}{\sigma}\right)\right]^{1/\xi}\right\} \quad (1)$$

where μ, σ, ξ are the location, scale and shape parameter respectively. According to Fisher and Tippett (1928), for $\xi = 0$ the distribution is called Gumbel; $\xi > 0$ refers to Fréchet and the $\xi < 0$ is corresponding to Weibull distribution (Coles, 2001). Several methods are developed to estimate the GEV model parameters, such as, Maximum Likelihood Estimation (MLE) (Smith, 1985), Probability Weighted Moment (Hosking et al., 1985), L-moments (Hosking, 1990), Method of Moments (Madsen et al., 1997) and Generalized Maximum Likelihood

Table 2
Stationary and Non-Stationary GEV models used in the study. [List of covariates: Year (Y); Daily maximum Temperature at time the event occurs (Tx); Annual mean Temperature (Tm); ENSO (E)].

Model	Formulation	Model	Formulation
S0	$GEV(\mu, \sigma, \xi)$		
NS1	$GEV((\mu_0 + Y\mu_1), \sigma, \xi)$	NS11	$GEV((\mu_0 + Y\mu_1 + Tm\mu_2 + E\mu_3), \sigma, \xi)$
NS2	$GEV((\mu_0 + Tx\mu_1), \sigma, \xi)$	NS12	$GEV((\mu_0 + Y\mu_1), e^{(\sigma_0+Y\sigma_1)}, \xi)$
NS3	$GEV((\mu_0 + E\mu_1), \sigma, \xi)$	NS13	$GEV((\mu_0 + Tx\mu_1), e^{(\sigma_0+Tx\sigma_1)}, \xi)$
NS4	$GEV((\mu_0 + Tm\mu_1), \sigma, \xi)$	NS14	$GEV((\mu_0 + E\mu_1), e^{(\sigma_0+E\sigma_1)}, \xi)$
NS5	$GEV((\mu_0 + Y\mu_1 + Tx\mu_2), \sigma, \xi)$	NS15	$GEV((\mu_0 + Tm\mu_1), e^{(\sigma_0+Tm\sigma_1)}, \xi)$
NS6	$GEV((\mu_0 + Y\mu_1 + E\mu_2), \sigma, \xi)$	NS16	$GEV((\mu_0 + Y\mu_1 + Tx\mu_2), e^{(\sigma_0+Y\sigma_1+Tx\sigma_2)}, \xi)$
NS7	$GEV((\mu_0 + Y\mu_1 + Tm\mu_2), \sigma, \xi)$	NS17	$GEV((\mu_0 + Y\mu_1 + Tm\mu_2), e^{(\sigma_0+Y\sigma_1+Tm\sigma_2)}, \xi)$
NS8	$GEV((\mu_0 + E\mu_1 + Tx\mu_2), \sigma, \xi)$	NS18	$GEV((\mu_0 + Y\mu_1 + E\mu_2), e^{(\sigma_0+T\sigma_1+E\sigma_2)}, \xi)$
NS9	$GEV((\mu_0 + E\mu_1 + Tm\mu_2), \sigma, \xi)$	NS19	$GEV((\mu_0 + Y\mu_1 + E\mu_2 + Tx\mu_3), e^{(\sigma_0+Y\sigma_1+E\sigma_2+Tx\sigma_3)}, \xi)$
NS10	$GEV((\mu_0 + Y\mu_1 + Tx\mu_2 + E\mu_3), \sigma, \xi)$	NS20	$GEV((\mu_0 + Y\mu_1 + E\mu_2 + Tm\mu_3), e^{(\sigma_0+Y\sigma_1+E\sigma_2+Tm\sigma_3)}, \xi)$

Estimators (Adlouni et al., 2007). In our study, we utilized the MLE method to estimate the GEV parameters for nonstationary analysis, and the similar method was applied in previous studies (Agilan and Umamahesh, 2017; Risser and Wehner, 2017, Mondal and Mujumdar, 2015). The conventional spatial bootstrap technique was applied for the significance test to determine the uncertainty bounds and also to estimate the return levels and the return periods.

3.2. Models and covariates

In the nonstationary analysis, the parameters are expressed as a function of covariates. As discussed earlier (Section 2.2), four covariates were selected for nonstationary analysis of extreme precipitation, which includes: (i) annual average daily temperature "Tm" (°C), (ii) the max daily temperature "Tx" (°C) recorded at the time the extreme events occurred, (iii) the seasonal average ERSST over Niño 3.4 region for the DJFM months to represent the influence of natural phenomenon "E", and (iv) time in year "Y". Different combinations of covariates are provided in Table 2. The Time-varying GEV distribution was applied by varying the location and scale parameters as a function of selected covariates. However, the shape parameter is kept constant as it may be unrealistic to assume shape parameter as a smooth function of time (Coles, 2001), and it is advisable to use the constant shape for a small number of stations (Cooley et al., 2007). Similar assumption has been made in recent studies (Sarhadi and Soulis, 2017; Risser and Wehner, 2017; Agilan and Umamahesh, 2017). For each of the couple station/duration, there are 21 models are derived, which includes, 1 stationary and 20 nonstationary models based on four covariates and two-time varying parameters. Overall, 18 best models were identified based on 378 models that were constructed based on a combination of 6 stations, three types of extreme events durations, and four types of covariates. A brief description of the model formulation is discussed here, and detailed information is provided in Table 2. Three model types are briefly discussed below:

Model type 1: Stationary model S0. Three GEV parameters are kept constant over time:

$$\mu_t = \mu;\ \sigma_t = \sigma;\ \xi_t = \xi \tag{2}$$

Model type 2: a Nonstationary model with varying location parameter with covariates NS1 to NS11 (Table 2), whereas, scale and shape parameters are kept constant over time.

$$\begin{aligned} \mu_t &= \mu_0 + \mu_1 Tm + \mu_2 Tx + \mu_3 E + \mu_4 Y \\ \sigma_t &= \sigma \\ \xi_t &= \xi \end{aligned} \tag{3}$$

Model type 3: a Nonstationary model with varying location and scale parameters based on covariates NS12 to NS20 (Table 2), whereas, shape parameter is kept constant over time.

$$\begin{aligned} \mu_t &= \mu_0 + \mu_1 Tm + \mu_2 Tx + \mu_3 E + \mu_4 Y \\ \log \sigma_t &= \sigma_0 + \sigma_1 Tm + \sigma_2 Tx + \sigma_3 E + \sigma_4 Y \\ \xi_t &= \xi \end{aligned} \tag{4}$$

The slope of μ_1, μ_2, μ_3, μ_4 represents the linear trend in location parameters, whereas the slope of σ_1, σ_2, σ_3, σ_4 demonstrating the linear trend in scale parameters respectively based on their associated covariates Tm (daily average temperature), Tx (daily max temperature), E (ENSO) and Y (Time domain).

3.3. Identification of the best models

The Akaike Information Criterion (AIC) was applied to identify the best model among 21 models (Table 2) for each station as well as different duration of extreme events. The model that has minimum AIC is selected as the best fit model (Makridakis et al., 2003). The mathematical equation for AIC is formulated as (Akaike, 1974):

$$AIC = -2\log L + 2m \tag{5}$$

where m is the number of terms estimated in the model; L is the likelihood function of the models with a monotonically decreasing function of the sum of squared residuals. The AIC penalizes the minimized negative log likelihood for the number of parameters estimated (Katz, 2013; Mishra and Desai, 2005). AIC is commonly used to select the best model, and it has been used for nonstationary analysis (Risser and Wehner, 2017; Agilan and Umamahesh, 2017; Mondal and Mujumdar, 2015).

The AIC values were computed for all the selected 21 models based on the 1-, 3-, 5-day annual maximum precipitation at six stations. The selected best model is then compared with stationary model S0 using the Likelihood Ratio test (LR) with 95% confidence intervals (Coles, 2001). If the test is insignificant, then the stationary model (S0) is considered as the best model. The best models based on the different types of extreme precipitation events at six locations are provided in Table 3.

Table 3
Selected models for the six stations based on three types of extreme rainfall events.

Station	1 day AMR	3 day AMR	5 day AMR
Fort Pierce	NS12	NS17	NS2
Houston AP	NS5	NS16	NS1
Barton Rouge AP	NS6	NS12	NS12
Charleston AP	S0	NS1	NS1
Boulder	NS11	NS6	NS2
Bayboro	NS12	NS3	S0

3.4. Estimation of the nonstationary return period

The nonstationary frequency analysis models were developed based on past observations by excluding the recent extreme event. For example, the historical AMR data was considered up to 2016 for model development for Fort Pierce station (hurricane Irma in 2017). Once the nonstationary models are identified, the return period for extreme events (e.g., hurricane Irma in 2017) are computed based on the model parameters based on the sets of the corresponding covariates (Tx, Tm, E, Y) of the current year. Once the best nonstationary model was identified, the corresponding return period for the recent extreme events was computed and compared with the corresponding return period from stationary GEV fitting. The formulation for the return period based on the stationary (nonstationary) model is given by the equation:

$$rp = \frac{1}{1 - \exp\left\{-\left[1 - \xi\left(\frac{z-\mu_t}{\sigma_t}\right)\right]^{1/\xi}\right\}} \quad (6)$$

where z is the corresponding AMR value of the extreme event, and μ_t, σ_t, ξ are the location, scale and shape parameters for corresponding nonstationary (stationary) models specified in equations (2), (3) and (4). The estimated model parameters and standard errors associated with the best models (Table 3) are provided in Table 4. The revised return periods for the most recent extreme precipitation events are provided in Table 5.

Finally, the change (%) in the return periods for the selected extreme events between nonstationary and stationary can be computed as in equation (7):

$$reduction = \frac{nrp - srp}{nrp} * 100(\%) \quad (7)$$

where *nrp* and *srp* represent the return periods based on the nonstationary and stationary approach.

4. Results

4.1. Nonstationary analysis and best covariates for selected models

The best models for the six selected stations are provided in Table 3, and their corresponding GEV parameters are tabulated in Table 4. Overall, 18 best models from 378 models are identified for three temporal precipitation durations at six locations. Out of these 18 best models, only 2 models follow stationary GEV (S0) and 16 models follow nonstationary processes. The nonstationary models vary based on their location and scale parameters due to the different potential influence of covariates.

The nonstationary models performed well based on all the AMR time series for the selected station located in Houston, Texas. It was observed that Clausius-Claperon relationship holds true for this location, where a strong relationship was observed between maximum daily temperature and extreme precipitation. Both the covariates (max daily temperature and Time) have a potential influence on the nonstationary nature (NS5 and NS16) of the 1- and 3-day AMR time series. It also implies that the change in temperature during the post-climatic period (1965-) (Mishra and Singh, 2010) has a potential influence on AMR. In

Table 4
GEV Parameter (μ,σ,ξ) estimated from different best models. (Type 'Est': Estimated GEV parameters; 'Err': Standard Error from the estimated parameters).

Station	AMR	Type	μ_0	μ_1	μ_2	μ_3	σ_0	σ_1	σ_2	σ_3	ξ
Fort Pierce	1-d AMR	Est	81.52	−1.70			28.19	−5.73			0.14
		Err	3.81	3.51			3.05	2.89			0.10
	3-d AMR	Est	124.17	−0.81	−5.05		42.96	12.03	5.77		−0.01
		Err	5.84	5.20	4.51		4.68	5.34	3.23		0.10
	5-d AMR	Est	140.08	−10.83			45.51				0.04
		Err	5.94	4.22			4.42				0.09
Houston	1-d AMR	Est	88.95	5.15	6.53		29.74				0.24
		Err	4.13	3.43	2.78		3.39				0.13
	3-d AMR	Est	128.85	15.60	5.17		48.23	−1.91	9.52		0.09
		Err	6.43	5.80	4.44		4.86	5.68	2.57		0.10
	5-d AMR	Est	141.93	16.57			52.71				0.13
		Err	6.60	6.02			4.95				0.07
Barton Rouge	1-d AMR	Est	92.05	11.92	8.04		24.50				0.16
		Err	3.03	2.59	2.65		2.30				0.08
	3-d AMR	Est	120.02	18.89			33.43	5.50			0.22
		Err	4.42	3.95			3.70	3.51			0.12
	5-d AMR	Est	134.21	16.61			38.72	5.74			0.13
		Err	5.13	4.53			4.08	3.93			0.12
Charleston	1-d AMR	Est	84.58				27.18				0.08
		Err	3.49				2.60				0.08
	3-d AMR	Est	117.24	3.74			31.94				0.06
		Err	4.04	3.78			2.96				0.08
	5-d AMR	Est	132.67	2.43			35.37				0.10
		Err	4.44	3.96			3.28				0.07
Boulder	1-d AMR	Est	37.22	3.12	−1.90	2.30	12.71				0.25
		Err	1.57	1.29	1.05	1.27	1.21				0.12
	3-d AMR	Est	50.23	3.59	2.70		16.43				0.25
		Err	2.02	1.58	1.54		1.57				0.12
	5-d AMR	Est	55.19	3.61			17.98				0.26
		Err	2.22	1.49			1.74				0.12
Bay Boro	1-d AMR	Est	83.94	10.54			24.58	2.33			0.10
		Err	4.85	5.07			3.29	3.80			0.15
	3-d AMR	Est	112.47	−9.12			36.79				0.04
		Err	6.41	5.82			4.73				0.12
	5-d AMR	Est	127.24				41.54				0.10
		Err	7.16				5.37				0.11

Table 5
Revised return period (year) based on nonstationary models for selected extreme rainfall.

Station	1 day AMR		3 day AMR		5 day AMR	
	Stationary model (Yr)	Nonstationary model (Yr)	Stationary model (Yr)	Nonstationary model (Yr)	Stationary model (Yr)	Nonstationary model (Yr)
Fort Pierce	228	156	6300	800	5370	3510
Houston	88	57	6726	4833	4947	3942
Barton Rouge	125	80	177	60	530	167
Charleston	400	–	1844	1062	718	594
Boulder	737	520	1132	850	1545	950
Bayboro	110	40	1570	1250	170	–

a recent study, Risser and Wehner (2017) highlighted that global warming is likely to increase the chances of the largest 7-day precipitation total by a factor of at least 3.5 for most of the affected areas in Houston. Based on the similar analysis over Fort Pierce station (FL), the average local temperature (Tm) and daily maximum temperature (Tx) are the most influencing covariates for nonstationary extreme precipitation analysis for the longer duration (3- and 5-days) AMR time series.

The nonstationary analysis for the Charleston station reveals that the 1-day AMR follows stationary processes (S0), however at longer duration, both 3- and 5-day AMR performed well by nonstationary models (NS1) based on time-varying location parameters. It implies that the stationary IDF curve best describes the 1-day AMR in Charleston, while for the 3-day and 5-day accumulated events, the nonstationary processes with time-varying location parameters are the best models to demonstrate the extreme precipitation behavior. In fact, the 5 days (October 1–5, 2015) accumulated precipitation led to a historic flooding event and flash flooding was prevalent that led to significant damage to civil infrastructure systems, and many people having to be rescued by emergency personnel.

Table 3 clearly demonstrates the potential influence of covariates on the nonstationary nature of extreme precipitation events in Baton Rouge, Lousiana. The best model identified for 1-day AMR is different from 3- and 5-day AMR. In this case, 3- and 5-day AMR follows similar nonstationary models based on varying location and scale parameters, whereas, time and ENSO found to be important covariates for 1-day AMR. In a recent study, Van der Wiel et al. (2017) highlighted that the return period of 3-day AMR event in Louisiana 2016 is about 550 years (with 95% confidence interval) and the intensity of extreme precipitation events of this return time have increased since 1900. Further, the authors suggested that the regional probability of 3-day extreme precipitation increases by more than a factor of 1.4 due to anthropogenic climate change. Our results point towards the potential influence of ENSO on extreme precipitation and Van der Wiel et al. (2017) highlighted that the evidence for a relation to El Niño half a year earlier can be possible with some analyses showing a positive connection and others none. Similarly, nonstationary models performed well for the other two stations located in Bay Boro station (North Carolina) and Boulder (Colorado). In the case of Boulder station, all the covariates contribute to the 1-day AMR, however, 5-day AMR at Bay Boro station followed a stationary model. In addition to that, the best models for 1- and 3-day AMR at Bay Boro station includes ENSO as potential covariates.

Overall most (16 out of 18) of the stations, as well as the duration of extreme precipitation, followed a nonstationary pattern. There are six best models follow the time-based covariates for location and scale parameters that represent 30% of the total number of models. Baton Rouge and Charleston are most likely Time based nonstationary models for higher durations (3- and 5-day extreme precipitation). About six models (30%) exhibit the significant relationship between combined covariates with extreme precipitation for shorter (1- and 3-day) duration. In general, for most of the locations, the frequency analysis of 5-day AMR show a significant relationship with only one covariate, and the choice of covariate varies for a different location. The GEV parameters estimated from different best models and their corresponding standard errors are provided in Table 4.

4.2. Revised return levels based on the nonstationary approach

The nonstationary frequency analysis was performed based on the available data prior to the occurrence of the recent extreme events. The corresponding return levels (periods) were computed based on the GEV parameters (Table 4) obtained from the nonstationary analysis of the best models. The nonstationary return levels based on 50-, 100- and 500-year return period using 3-day AMR data sets for the best models are provided in Fig. 4. It can be observed that the nonstationary return levels vary with time in contrast to the stationary return level.

The time-varying covariate in location parameter (model NS1, Charleston – Fig. 4d) indicates return levels with a linear pattern having a mild slope along the time domain. In the case of time-varying location and scale varying parameters (NS12 model; Fig. 4c), the corresponding return level witness a moderate slope based on the linear return levels. The steep slopes associated with return levels (Fig. 4c) indicates the reduction in return period with respect to recent time periods. In other word, the large magnitude of storms is becoming more common in recent times (Risser and Wehner, 2017).

The return level patterns likely to be influenced by the type of covariates. The oscillating pattern of non-stationary return levels depends on the choice of covariates. For example, the return levels with ENSO as a covariate (NS3; Fig. 4f) fluctuates with the variation of SST unlike the linear increasing trend observed based on the Time covariate. A similar observation was made based on the Time and ENSO covariates (model NS6) for Boulder station (Fig. 4e). It was observed that the return levels associated with ENSO covariate may not follow a significant increasing or decreasing trend. The best model for Fort Pierce station (NS17; Fig. 4b) incorporates Time and mean temperature as covariates that result in significant increasing trends for all the return periods. It is slightly different from Fig. 4c, where only Time covariate was considered. The oscillation of the return level is due to the effect of mean temperature covariates. It is worth to highlight that the 3-day maximum AMR extreme event precipitation (570 mm) recorded during hurricane Irma at Fort Pierce (Fig. 4b) represents 500 year return period based on the nonstationary analysis, however, this return period is comparatively higher based on the stationary analysis. The recorded 3-day AMR event from hurricane Harvey (Fig. 4a) is higher than 500 year return period based on the nonstationary process (NS16 model) that includes Time and maximum temperature as covariates along with location and scale parameters.

Overall, it was observed that the temporal pattern of return levels varies with the covariates. Some of the covariates may lead to a linearly increasing trend (e.g., time and land use change due to urbanization) in nonstationary return level. Whereas, some of the covariates (e.g., maximum daily temperature and ENSO) likely to oscillate with no clear pattern of increasing (decreasing) trend may induce similar behavior with return levels as well. However, the combination of time and other covariates, for example, ENSO (NS6) and mean temperature (NS17)

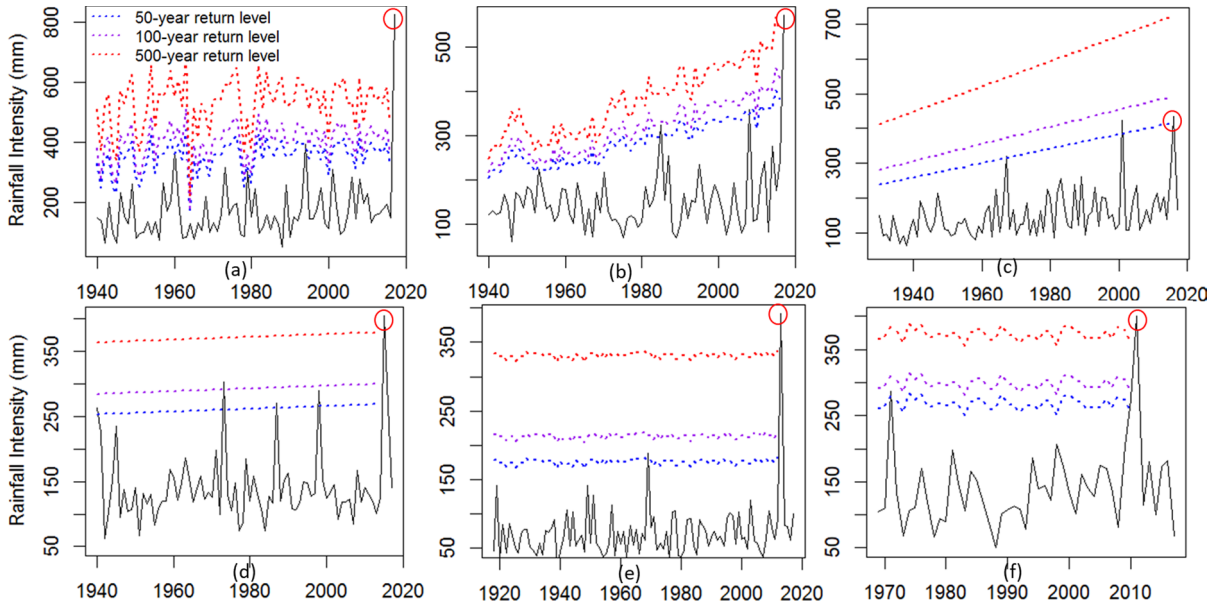

Fig. 4. Nonstationary Return Levels based on 3-day AMR corresponding to 50-, 100-, 500-year return period based on best models for: (a) Houston-NS16; (b) Fort Pierce-NS17; (c) Baton Rouge-NS12; (d) Charleston-NS1; (e) Boulder-NS6; (f) BayBoro-NS3. [Note: The continuous black line indicates the 3 day AMR timeseries and the recent extreme events are highlighted in red circles]. (For interpretation of the references to colour in this figure legend, the reader is referred to the web version of this article.)

may result in an increase in the return level trend (Fig. 4c and 3f) respectively.

The return level and return period are estimated for each studied station for 1-day, 3-day, and 5-day AMR. Fig. 5 demonstrates the nonstationary return level for 3-day AMR time series based on 500 year return period along with its uncertainty. The continuous red line represents the return level based on a 500-year return period, and the green and blue bands exhibit the 60% and 95% confidence intervals respectively, and they are computed using the bootstrapping technique. The 95% confidence interval (compared to 60%) indicates a steady increasing trend for Fort Pierce, Baton Rouge and Charleston (Fig. 5b, c, d).

4.3. Intensity duration frequency curve from nonstationary analysis

Fig. 6 compares the stationary and nonstationary intensity duration frequency (IDF) curves derived based on the best model parameters (Table 4). The recent extreme precipitation events were compared against IDF curves as shown in Fig. 6. The nonstationary IDF curves were derived based on the best models that include Time covariate

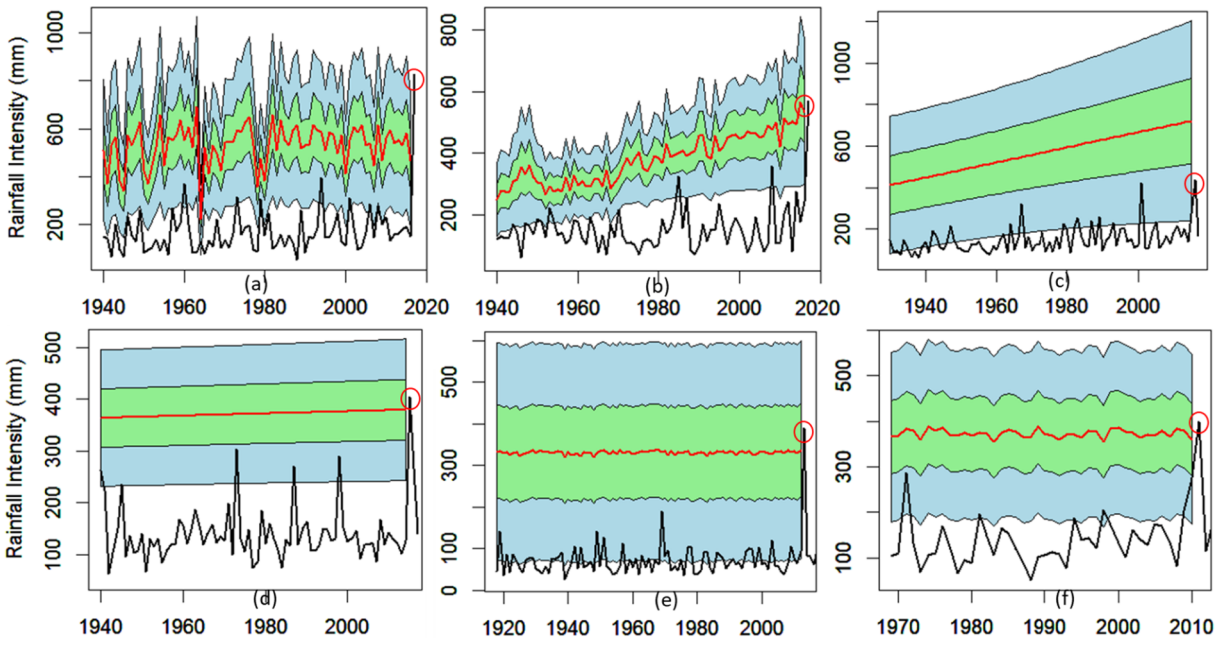

Fig. 5. Nonstationary Return level (3-day AMR) for 500-year return period with 60% (green band) and 95% (blue band) confidence intervals by excluding the recent extreme events (circled) (a) Houston-NS16; (b) Fort Pierce-NS17; (c) Baton Rouge-NS12; (d) Charleston-NS1; (e) Boulder-NS6; (f) BayBoro-NS3 [Note: Solid black line represents the 3-day AMR over different years and the recent extreme event highlighted by the red circle]. (For interpretation of the references to colour in this figure legend, the reader is referred to the web version of this article.)

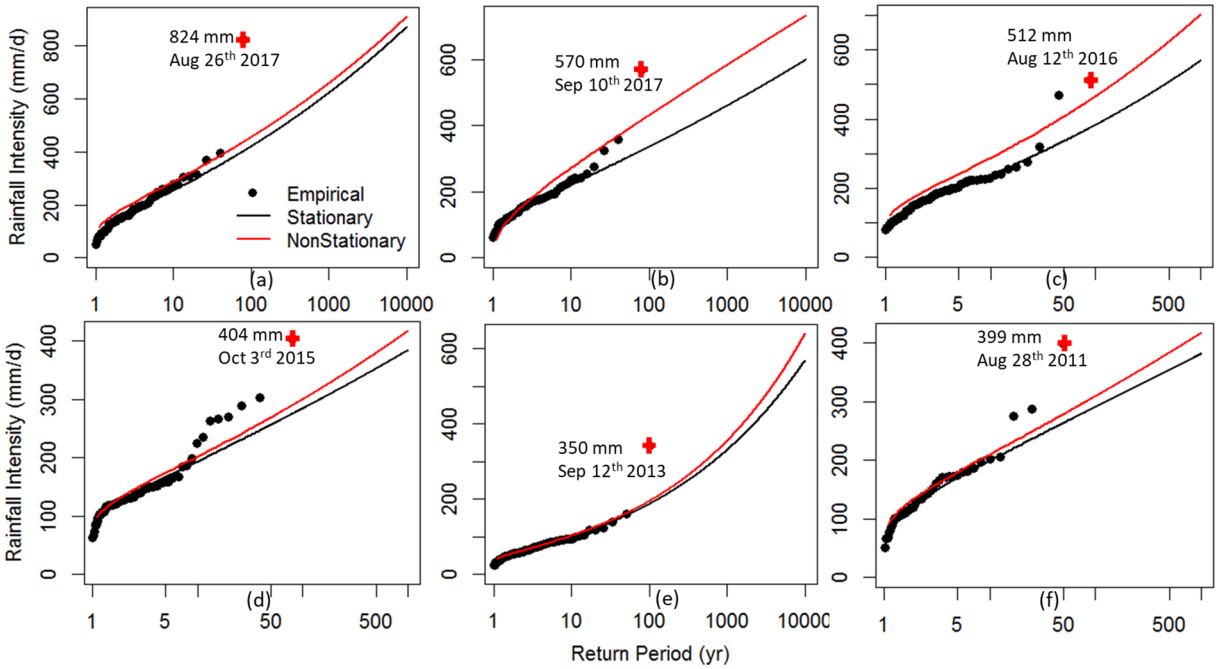

Fig. 6. Intensity-Duration-Frequency curve using AMR3-day max precipitaiton: (a) Houston (NS16 model); (b) Fort Pierce (NS17 model); (c) Barton Rouge (NS12 model); (d) Charleston (NS1 model); (e) Boulder (NS6 model); (f) BayBoro (NS3 model). [Note: The black and red solid lines represents stationary and nonstationary IDF curves respectively, and recent extreme events are represented by red cross] (For interpretation of the references to colour in this figure legend, the reader is referred to the web version of this article.)

(Fig. 6c, d), maximum daily temperature and ENSO (Fig. 6a), Time and ENSO (Fig. 6e), Time and mean temperature (Fig. 6b) and ENSO only (Fig. 6f). It was observed that the nonstationary curves (red lines) are always higher than a stationary one (black lines), which suggests that the nonstationary models represent a reduced return period compared to the stationary ones.

Revised return periods for different temporal resolutions based on the stationary and nonstationary frequency analysis are provided in Table 5. It was observed that the magnitude of return periods of extreme event reduced significantly from stationary to the nonstationary case. For example, the amount of aggregated precipitation based on 3 and 5-days precipitation due to hurricane Harvey (Houston station) represents a return period of approximate 6700 and 5000 years respectively based on the stationary assumption. These extremely high return periods are also highlighted in the literature by Risser and Wehner (2017) and Emanuel (2017). However, based on the nonstationary analysis, the return period for these extreme events reduced to 4800 and 3900 years (reduced by 30% and 25%) respectively. In the case of Hurricane Irma (Fort Pierce, FL), the return periods based on the stationary assumption for 3-day AMR and 5-day AMR are close to 6300 and 5370 years respectively, these numbers reduce to 800 and 3500 years (87% and 35%) based on the nonstationary analysis. It is important to highlight that the 5000 year return period of extreme precipitation does not correspond to the 5000 year return period of the flood event (Gochis et al., 2015). Similarly, the return periods for other stations (Charleston, Boulder, and Bayboro) are also greater than thousand years based on the 3-day AMR (Table 5). The extreme precipitation events at different time scales witness a reduction in the return period based on the nonstationary GEV analysis.

The percentage reduction in the return periods for all selected extreme events computed from nonstationary and stationary models as formulated in equation (7) shown in Fig. 7. All the nonstationary models exhibit a reduction in the return period compared to the stationary model that ranges from the lowest rate of 17% to the highest rate of 87%. The study clearly highlights that the occurrence of similar extreme precipitation events likely to be more frequent when the return periods are reduced based on the nonstationary analysis. For example, the return period of 3-day extreme events at Barton Rogue reduced from 177 to 60 years based on the nonstationary analysis. This does not mean that the two extreme events will not occur in a short period of time. For example, two severe most hurricanes (Harvey and Irma) occurred in a month in 2017. It is important to highlight that the percentage change between stationary and nonstationary return periods is not consistent among temporal resolutions (i.e., 1, 3, 5 days), and they vary at different locations. However, some of the prominent changes were observed for coastal locations with respect to recent extreme events, for example, Baton Rouge (66 and 68%) based on the 3 and 5 days events; Fort Pierce (87%) based on the 3 day extreme events, and Bay Boro (64%) based on the 1 day extreme events.

5. Discussion and conclusion

One of the key information required to design major civil infrastructure systems includes intensity, duration, and frequency of heavy precipitation events. These precipitation characteristics are combined to construct Intensity-Duration-Frequency (IDF) curves, which are typically derived based on the stationary assumption. The IDF curves are widely used for designing civil infrastructure systems, for example, designing of hydraulic structures against the impact of extreme events (e.g., extreme precipitation, floods). The models used to derive return periods (i.e., frequency analysis) are generally developed based on the assumption that hydrological events (e.g., annual maximum rainfall and flood discharges) arise from a stationary hydrological regime. However, it has been reported in the literature that the hydrological cycle has been changing leading to significant changes in the spatio-temporal distribution of occurrences of extreme events. Thus, there is a need to revisit IDF curves as well as to develop new methods where there is sufficient evidence of nonstationarity. In addition, the selection of return periods depend on additional variables such as cost of damages, vulnerability and climate risk, that needs to be incorporated to develop economic risk-based decision approach. This is specifically important for countries frequently affected by the severe storm events,

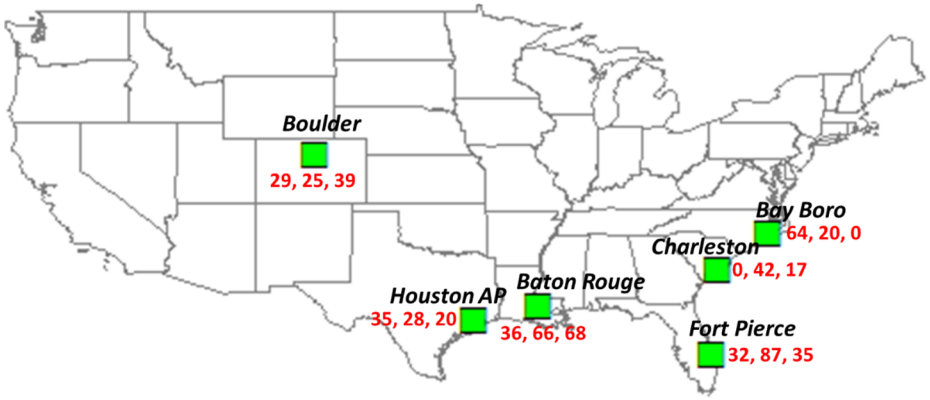

Fig. 7. The percentage reduction in the return periods for all selected extreme events computed from nonstationary and stationary models (The red numbers in each station demonstrate the reduction (%) in return period for AMR1, AMR3 and AMR5 respectively for the historic storms). (For interpretation of the references to colour in this figure legend, the reader is referred to the web version of this article.)

for example, in Singapore the IDF curves are typically updated once per decade (Singapore PUB, 2012) to cope up with the changing climate condition in order to improve the resilience of infrastructure systems. The nonstationary IDF curves can be explored during the design phase of the infrastructure in order to evaluate the cost and benefit with respect to stationary IDF curves (especially when these curves are not updated recently).

In this study, we performed the nonstationary frequency analysis of the most recent historical precipitation events occurred between 2011 and 2017 over the United States. Overall, six extreme precipitation events are selected and their corresponding AMR time series are constructed based on annual maximum 1, 3 and 5 days aggregated values. The return period of extreme precipitation events are likely to be influenced by the occurrence of the extreme events within a short period of time, for example, two “thousand year return period” precipitation extreme events occurred (hurricane Harvey and Irma) in 2017. The following conclusions can be drawn from this study.

(a) While the stationary frequency analysis is commonly used for civil infrastructure design, recently multiple studies highlighted the increase in the nonstationary pattern of extreme events. In this study, we performed stationary (nonstationary) frequency based on six extreme precipitation events during the period 2011–2017. Overall, 378 stationary (nonstationary) models were evaluated for three types (1-, 3-, 5- day AMR) of extreme precipitation events at six locations and 18 best models were identified. It was observed that most (approx 90%) of the extreme precipitation events follow the nonstationary pattern over the selected time period. This may be due to the increase in the magnitude of recent extreme precipitation events, especially during hurricane events.

(b) The selection of physical covariates is an important step for nonstationary frequency analysis. Overall, four distinct covariates are identified for nonstationary frequency analysis, which includes large-scale climate index (ENSO), time covariate, local annual average temperature and maximum daily temperature during the occurrence of the events. Different combination of covariates can potentially influence the nonstationary frequency analysis, therefore sensitivity test is an important step to identify best covariates. Different combination of covariates is evaluated for a different type of extreme precipitation patterns at six locations witnessing different climate patterns. It was observed that there is not a single covariate that is most sensitive to the nonstationary frequency analysis in all of the cases. In fact, the combination of several covariates can perform better than using a single covariate. For example, 1-day AMR time series followed a stationary pattern and time-varying covariate for 3-day and 5-day AMR time series. All other stations/durations have a different combination of covariates.

(c) The temporal pattern of nonstationary return level depends on the extreme value distribution parameters (e.g., location and scale parameters) and the choice of covariates. For example, based on the time covariate (e.g., NS1 and NS12 model), a linearly increasing trend may be expected for nonstationary return level, whereas, the return levels based on ENSO and temperature likely to oscillate over time compared to Time covariate. This is due to the temporal variation of the Sea Surface Temperature and change in local temperature over a period of time. Therefore more studies are necessary to quantify the potential physical mechanism between extreme events and corresponding influencing variables.

(d) Using the best nonstationary models, the Intensity Duration Frequency curves were constructed based on the combination of 6 stations and 3 durations for comparison with stationary IDF curves. Based on the Nonstationary Extreme Value Analysis, the return periods associated with extreme precipitation events significantly reduced compared to the stationary approach. Although six representative extreme events at 3 different temporal resolutions (1-, 3- and 5-day consecutive) are selected in this analysis, an additional number of events can be investigated in the future research by incorporating more number of precipitation stations to quantify the heterogeneous nature of events within a spatial domain. In the process of choosing more number of stations for a particular event may lead to a different set of model parameters and covariates, and such analysis is required to investigate the extreme events at a regional scale.

(e) The extreme precipitations events are often associated with hurricanes and tropical storms in the US. Therefore, in addition to annual maxima approach discussed in this study, additional extreme value distribution (such as Generalized Pareto) can be applied to Peak Over Threshold (POT) data set to capture various extreme precipitation events that occurred within the year. Further, the return periods based on the nonstationary model can be influenced by data length, parameter estimation techniques as well as the type of the covariates. Therefore, in-depth analysis is further required to minimize the uncertainty associated with such influencing variables.

Declaration of Competing Interest

We have no conflict of interest to report.

Acknowledgement

We very much appreciate the editor and reviewer’s critical and valuable comment that helped us to improve the manuscript. This study was supported by the United States National Science Foundation (NSF) award # 1855374.

References

Adlouni, S.E., Ouarda, T.B.M.J., Zhang, X., Roy, R., Bobée, B., 2007. Generalized maximum likelihood estimators for the nonstationary generalized extreme value model.

Water Resour. Res. 43, W03410. https://doi.org/10.1029/2005WR004545.
Agilan, V., Umamahesh, N.V., 2017. What are the best covariates for developing non-stationary precipitation Intensity-Duration-Frequency relationship? Adv. Water Resour. 101, 11–22.
Akaike, H., 1974. Markovian representation of stochastic processes and its application to the analysis of autoregressive moving average processes. Annals Ins. Stat. Math. 26, 363–387.
Aon. 2018. Hurricane Irma Event Recap Report. http://thoughtleadership.aonbenfield.com/Documents/20180328-ab-if-hurricane-maria-recap.pdf (Last accessed: 11/2018).
Bracken, C., Rajagopalan, B., Alexander, M., Gangopadhyay, S., 2015. Spatial variability of seasonal extreme precipitation in the western United States. J. Geophys. Res.: Atm. 120, 4522–4533. https://doi.org/10.1002/2015JD023205.
Cheng, L., AghaKhouchak, A., 2014. Nonstationary precipitation intensity-duration-frequency curves for infrastructure design in a changing climate. Scientific Report 4, 7093. https://doi.org/10.1038/srep07093.
Coles, G.S., 2001. An Introduction to Statistical Modeling of Extreme Values 208 Springer, New York.
Condon, L.E., Gangopadhyay, S., Pruitt, T., 2015. Climate change and non-stationary flood risk for the upper Truckee River basin. Hydrol. Earth Sys. Sci. 19, 159–175.
Cooley, D., Nychka, D., Naveau, P., 2007. Bayesian spatial modeling of extreme precipitation return levels. J. Am. Stat. Assoc. 102 (479), 824–840. https://doi.org/10.1198/016214506000000780.
Daly, C., Neilson, R.P., Phillips, D.L., 1994. A statistical-topographic model for mapping climatological precipitation over mountainous terrain. J. Appl. Meteor. 33, 140–158.
Donat, M., Lowry, A., Alexander, L., O'Gorman, P., Maher, N., 2016. More extreme precipitation in the world's dry and wet regions. Nat. Clim. Chang. 6, 508–513.
Degu, A.M., Hossain, F., Niyogi, D., Pielke Sr., R., Shepherd, J.M., Voisin, N., Chronis, T., 2011. The influence of large dams on surrounding climate and precipitation patterns. Geophys. Res. Lett. 38, L04405. https://doi.org/10.1029/2010GL046482.
Deflorio, M.J., Pierce, D.W., Cayan, D.R., Miller, A.J., 2013. Western U.S. extreme precipitation events and their relation to ENSO and PDO in CCSM4. J. Clim. 26, 4231–4243.
Editorial, 2017. Storms ahead. Nat. Clim. Change 7, 671. https://doi.org/10.1038/nclimate3415.
Ellenrieder, T., 2018. Hurricane Harvey: Record-breaking floods inundate Houston. Munich Re Report. https://www.munichre.com/topics-online/en/2017/12/hurricane-harvey. (Last Accessed: 11/2018).
Emanuel, K., 2017. Assessing the present and future probability of Hurricane Harvey's precipitation. Proc. Nat. Acad. Sci. 1–4. https://doi.org/10.1073/pnas.1716222114.
Fisher, R.A., Tippett, L.H.C., 1928. Limiting forms of the frequency distribution of the largest or smallest members of a sample. Proc. Cambridge Philos. Soc. 24, 180–190.
Gershunov, A., Barnett, T.P., 1998. ENSO influence on intraseasonal extreme precipitation and temperature frequencies in the contiguous United States: observations and model results. J. Clim. 11 (7), 1575–1586.
Gochis, D., Schumacher, R., Friedrich, K., Doesken, N., Kelsch, M., Sun, J., Ikeda, K., Lindsey, D., Wood, A., Dolan, B., 2015. The great Colorado flood of September 2013. Bull. Am. Met. Soc. 96 (9), 1461–1487.
Hanley, D.E., Bourassa, M.A., O'Brien, J.J., Smith, S.R., Spade, E.R., 2003. A quantitative evaluation of ENSO indices. J. Clim. 16, 1249–1258.
Herath, S.M., Sarukkaligea, R., Nguyen, V.T.V., 2018. Evaluation of empirical relationships between extreme precipitation and daily maximum temperature in Australia. J. Hydrol. 556, 1171–1181.
Hosking, J.R.M., 1990. L-moment-analysis and estimation of distributions using linear combinations of order statistics. J. R. Stat. Soc. B 52, 105–124.
Hosking, J.R.M., Wallis, J.R., Wood, E.F., 1985. Estimation of the generalized extreme-value distribution by the method of probability weighted moments. Technometrics 27, 251–261.
Huang, H., Winter, J.M., Osterberg, E.C., 2018. Mechanisms of abrupt extreme precipitation change over the Northeastern United States. J. Geophys. Res. 123 (14), 7179–7192. https://doi.org/10.1029/2017JD028136.
Ivancic, T.J., Shaw, S.B., 2016. A U.S.-based analysis of the ability of the Clausius-Clapeyron relationship to explain changes in extreme precipitation with changing temperature. J. Geophys. Res. Atmos. 121, 3066–3078. https://doi.org/10.1002/2015JD024288.
Jenkinson, A.F., 1955. The frequency distribution of the annual maximum (or minimum) values of meteorological elements. Quar. J. Royal Met. Soc. 81, 58–171.
Kaplan, A., Cane, M., Kushnir, Y., Clement, A., Blumenthal, M., Rajagopalan, B., 1998. Analyses of global sea surface temperature 1856–1991. J. Geophys. Res. 103, 18567–18589.
Katz, R.W., 2009. Statistics of extremes in climate change. Clim. Change 100, 71–76.
Katz, R.W., 2013. Statistical methods for nonstationary extremes. In: Extremes in a Changing Climate: Detection, Analysis and Uncertainty. Springer, Dordrecht, pp. 15–37.
Konapala, G., Mishra, A., Leung, L.R., 2017. Changes in temporal variability of precipitation over land due to anthropogenic forcings. Environ. Res. Lett. 12 (2), 024009.
Kunkel, E.K., et al., 2008. Observed changes in weather and climate extremes. Weather and Climate Extremes in a Changing Climate. Regions of Focus: North America, Hawaii, Caribbean, and U.S. Pacific Islands, T. R. Karl et al., Eds., U.S. Climate Change Science Program and the Subcommittee on Global Change Research Rep., 35–80. [https://www.climatecommunication.org/wp-content/uploads/2012/01/climateextremes.pdf] (Last Access: Dec 2018).
Kunkel, E.K., et al., 2013. Monitoring and understanding trends in extreme storms: state of knowledge. Bull. Am. Meteor. Soc. 499–514.
Leng, Z., Leung, R.B., Hagos, S., Houze, R.A., Burleson, C.D., Balaguru, K., 2016. More frequent intense and long-lived storms dominate the springtime trend in central US precipitation. Nat. Comm. 7, 13429. https://doi.org/10.1038/ncomms13429.
Luong, M.T., Castro, C.L., Chang, H., Lahmers, T., Adams, D.K., Ochoa-Moya, C.A., 2017. The more extreme nature of North American monsoon precipitation in the Southwestern United States as revealed by a historical climatology of simulated severe weather events. J. Appl. Met. Clim. 56, 2509–2529. https://doi.org/10.1175/JAMC-D-16-0358.1.
Madsen, H., Rasmussen, P.F., Rosbjerg, D., 1997. Comparison of annual maximum series and partial duration series methods for modeling extreme hydrologic events: 1. At-site modeling. Water Resour. Res. 33, 747–758.
Makridakis, S., Wheelwright, S.C., Hyndman, R., 2003. Forecasting Methods and Applications. Wiley (ASIA) Pvt Ltd., Singapore.
Marciano, C.G., Lackmann, G.M., 2017. The South Carolina flood of october 2015: moisture transport analysis and the role of hurricane joaquin. J. Hydrometeor. 18, 2973–2990. https://doi.org/10.1175/JHM-D-16-0235.1.
Mason, S.J., Goddard, L., 2001. Probabilistic precipitation anomalies associated with ENSO. Bull. Am Met. Soc. 82 (4), 619–638.
Milly, P.C.D., Betancourt, J., Falkenmark, M., Hirsch, R.M., Kundzewicz, Z.W., Lettenmaier, D.P., Stouffer, R.J., 2008. Stationarity is dead: whither water management? Science 319, 573–574. https://doi.org/10.1126/science.1151915.
Mishra, A.K., Singh, V.P., 2010. Changes in extreme precipitation in Texas. J. Geophys. Res 15, D14106. https://doi.org/10.1029/2009JD013398.
Mishra, A.K., Özger, M., Singh, V.P., 2009. An entropy-based investigation into the variability of precipitation. J. Hydrol. 370, 139–154.
Mishra, A.K., Desai, V.R., 2005. Drought forecasting using stochastic models. Stoch. Environ. Res. Ris. Assess. 19 (5), 326–339. https://doi.org/10.1007/s00477-005-0238-4.
Mizzell, H., Malsick, M., Tyler, W., 2016. The historic south carolina precipitation and major floods of october 1–5, 2015. J. South Carolina Water Res. 3 (1), 3–7.
Mondal, A., Mujumdar, P.P., 2015. Modeling non-stationarity in intensity, duration and frequency of extreme precipitation over India. J. Hydrol. 521, 217–231.
Neelin, J.D., Sahany, S., Stechmann, S.N., Bernstein, D.N., 2017. Global warming precipitation accumulation increases above the current-climate cutoff scale. Proc. Nat. Acad. Sci. 114 (6), 1258–1263. https://doi.org/10.1073/pnas.1615333114.
NOAA, National Centers for Environmental Information (NCEI) U.S. Billion-Dollar Weather and Climate Disasters (2019). https://www.ncdc.noaa.gov/billions/ (Last accessed Feb 2019).
NWS, 2016. Exceedance Probability Analysis for the Louisiana Precipitation Event, 11-13 August 2016. http://www.nws.noaa.gov/oh/hdsc/aep_storm_analysis/AEP_Louisiana_August2016.pdf (Last Access: Jan 2019).
NWS, 2013a: Exceedance probability analysis for the Colorado flood event, 9–16 September 2013. Hydrometeorological Design Studies Center Rep., 5 pp. www.nws.noaa.gov/oh/hdsc/aep_storm_analysis/8_Colorado_2013.pdf. (Last Access: Jan 2019).
O'Gorman, P.A., Schneider, T., 2009. The physical basis for increases in precipitation extremes in simulations of 21st-century climate change. Proc. Nat. Acad. Sci. 106 (35), 14773–14777. https://doi.org/10.1073/pnas.0907610106.
Pfahl, S., O'Gorman, S.A., Fischer, E.M., 2017. Understanding the regional pattern of projected future changes in extreme precipitation. Nat. Climate change 7, 423–427. https://doi.org/10.1038/nclimate3287.
Risser, M.D., Wehner, M.F., 2017. Attributable human-induced changes in the likelihood and magnitude of the observed extreme precipitation during hurricane harvey. Geo. Res. Lett. 44, 12457–12464.
Romero, Y.L., Bessembinder, J., van de Giesen, N.C., van de Ven, F.H.M., 2011. A relation between extreme daily precipitation and extreme short-term precipitation. Clim. Change 106, 393–405.
Samenow, J., 2016. No-name storm dumped three times as much rain in Louisiana as Hurricane Katrina. The Washington Post. https://www.washingtonpost.com/news/capital-weather-gang/wp/2016/08/19/no-name-storm-dumped-three-times-as-much-rain-in-louisiana-as-hurricane-katrina/?noredirect=on&utm_term=.c8d9b5c3585a. (Last Accessed 11/2018).
Sarhadi, A., Soulis, E.D., 2017. Time-varying extreme precipitation intensity-duration-frequency curves in a changing climate. J. Geophys. Res 44, 2454–2463. https://doi.org/10.1002/2016GL072201.
Schubert, S.D., Chang, Y., Suarez, M.J., Pegion, P.J., 2008. ENSO and wintertime extreme precipitation events over the contiguous United States. J. Clim. 21, 22–39.
Smith, A.B., Katz, R.W., 2013. US billion-dollar weather and climate disasters: data sources, trends, accuracy and biases. Nat. Hazards 67 (2), 387–410.
Smith, R.L., 1985. Maximum likelihood estimation in a class of nonregular cases. Biometrika 72, 67–92.
Singapore Public Utilities Board (PUB). 2012. Report on Key Conclusions and Recommendations of the Expert Panel on Drainage Design and Flood Protection Measures. (https://www.pub.gov.sg/Documents/fullReport.pdf). Last Accessed: 04/2019.
Son, C., Lee, T., Kwon, H.-H., 2017. Integrating nonstationary behaviors of the typhoon and non-typhoon extreme precipitation events in East Asia. Scientific Report 7, 5097. https://doi.org/10.1038/s41598-017-04629-1.
Suro, T.P., Roland, M.A., Kiah, R.G., 2011. Flooding in the Northeastern United States 2011. USGS Professional Paper 1821, 42pp.
van der Wiel, K., Kapnick, S.B., van Oldenborgh, G.J., Whan, K., et al., 2017. Rapid attribution of the August 2016 flood-inducing extreme precipitation in south Louisiana to climate change. Hydrol. Earth Syst. Sci. 21, 897–921.
Vasiliades, L., Galiatsatou, P., Loukas, A., 2015. Nonstationary frequency analysis of annual maximum precipitation using climate covariates. Water Resour. Manage. 29, 339–358.
Villarini, G., Smith, J.A., Serinaldi, F., Bales, J., Bates, P.D., Krajewski, W.F., 2009. Flood

frequency analysis for nonstationary annual peak records in an urban drainage basin. Adv. Water Resour. 32 (8), 1255–1266. https://doi.org/10.1016/j.advwatres.2009.05.003.

Westra, S., Fowler, H.J., Evans, J.P., Alexander, L.V., Berg, P., Johnson, F., Kendon, E.J., Lenderink, G., Roberts, N.M., 2014. Future changes to the intensity and frequency of short-duration extreme precipitation. Rev. Geophys. 52 (3), 522–555.

Wi, S., Valdes, J.B., Steinschneider, S., Kim, T.-W., 2016. Non-stationary frequency analysis of extreme precipitation in South Korea using peaks-over-threshold and annual maxima. Stoch. Environ. Res. Risk Assess. 30 (2), 583–606. https://doi.org/10.1007/s00477-015-1180-8.

Yochum, S.E., Moore, D.S. 2013, Colorado Front Range Flood of 2013: Peak flow estimates at selected mountain stream locations. U.S. Department of Agriculture, Natural Resources Conservation Service, Colorado State Office, doi: 10.13140/2.1.2593.0242.

Yu, L., Heilman, W.E., Zhong, S., Bian, X., 2017. Relationships of the symmetric and asymmetric components of ENSO to US extreme precipitation. Atmos. Sci. Lett. 18 (12), 466–474. https://doi.org/10.1002/asl.790.